ADVANCED MATERIALS

Supporting Information

for *Adv. Mater.*, DOI: 10.1002/adma.202000801

Memristive Behavior Enabled by Amorphous–Crystalline 2D Oxide Heterostructure

*Xin Yin, Yizhan Wang, Tzu-hsuan Chang, Pei Zhang, Jun Li, Panpan Xue, Yin Long, J. Leon Shohet, Paul M. Voyles, Zhenqiang Ma, and Xudong Wang**

Supporting Information

Memristive Behavior Enabled by Amorphous-Crystalline Two Dimensional Oxide Heterostructure

*Xin Yin, Yizhan Wang, Tzu-hsuan Chang, Pei Zhang, Jun Li, Panpan Xue, Yin Long, J. Leon Shohet, Paul M. Voyles, Zhenqiang Ma, Xudong Wang**

S1. Experiment section

ZnO nanosheets were synthesized at water-air interface by our reported method.[1] 1 cm x 1 cm SiO_2 (thickness: 50 nm) coated Si substrate was used to transfer the ZnO nanosheets by scooping at the surface of the solution, *i.e.*, simply dipping the substrate into the solution and then lifting. Excess liquid was immediately removed from the substrate surface by filter paper absorption, and then dried at room temperature in controlled environment.

S1.2. Characterization

A Zeiss LEO 1530 field-emission scanning electron microscope was used to study the morphologies of the nanosheets. Atomic force microscopy (AFM) tomography images were obtained using an XE-70 Park System. X-ray photoelectron spectroscopy (XPS) spectrum was obtained from a Thermo Scientific K-alpha XPS instrument with a 100 μm spot size, with the flood gun turned on during the measurements. An FEI TF30 transmission electron microscope operated at 300 kV was used to study the crystal structure. The energy-dispersive X-ray spectrum (EDX) and electron energy loss spectroscopy (EELS) were measured using the STEM mode on a probe aberration corrected FEI Titan operating at 200 kV.

Memristive behavior was measured on HP 4155b semiconductor-parameter analyzer. DS345 Functional Generation was used to generate the pulse. Each pulse lasted 0.01 seconds and is composed of a set-reset pulse of 420 ns with pulses of 0, 10, 0, -8, and 0 V. The voltage was applied to the device for 50 seconds, and then the current was measured using HP 4155b with pulse 0.25 V.[2]

S1.3 Memristor device fabrication

The ZnO nanosheets were transferred to a Si substrate with 50 nm thermal oxide layer at the top. The samples were then annealed at 400 °C and 50 Pa for 1 hour in Ar atmosphere to remove residues from the solution-based synthesis. After annealing, the Ti/Au electrodes were deposited by e-beam evaporation with the usage of a shadow mask to form Au-ZnO-Au (MIM) devices. The purpose of using this direct deposition method for electrodes fabrication was to minimize the damage and surface contamination of the atomically thin ZnO nanosheets during the fabrication process. Due to the reactive oxide surface and ultrasmall thickness, the traditional e-beam lithography (e-beam writing/wet etch cycles) could introduce severe surface contamination and damage the nanosheets and interface. Finally, a 5-nm thin amorphous Al_2O_3 layer was then deposited on the surface of the entire ZnO nanosheet device by atomic layer deposition (ALD). ALD coating was performed in a home-made ALD system. The target substrate was loaded on a quartz tube and placed at the position 5 cm away from the precursor inlet nozzle. N_2 gas with a flow rate of 40 sccm was introduced into the chamber to serve as the carrier gas. The system's base pressure was kept at 0.36 Torr. The chamber temperature was maintained at 150 °C for the experiment. Trimethylaluminum (TMA) and DI H_2O vapors were pulsed into the deposition chamber separately with a pulsing time of 0.5 s and separated by 60 s N_2 purging. Therefore, one deposition cycles involve 0.5 s of H_2O pulse + 60 s of N_2 purging + 0.5 s of TMA pulse + 60 s of N_2 purging with a TMA pressure change of 140 millitorr (chamber pressure difference before and after ALD valve open). The chamber was cooled down naturally under N_2 flow after growth. 5 nm-thick Al_2O_3 coatings were received after 50 ALD cycles, corresponding to a growth rate of 0.1 nm per cycle.

The as-transferred ZnO sample was annealed at 400 °C under Ar to remove possible organic residues before Al_2O_3 coating. SEM, AFM and HRTEM analyses confirmed the surfaces of ZnO nanosheets were smooth and clean. The sharp ZnO/Al_2O_3 interfaces were confirmed by cross-sectional TEM images, STEM element mapping, and the XPS depth profile.

S2. SEM images and AFM characterization of the devices.

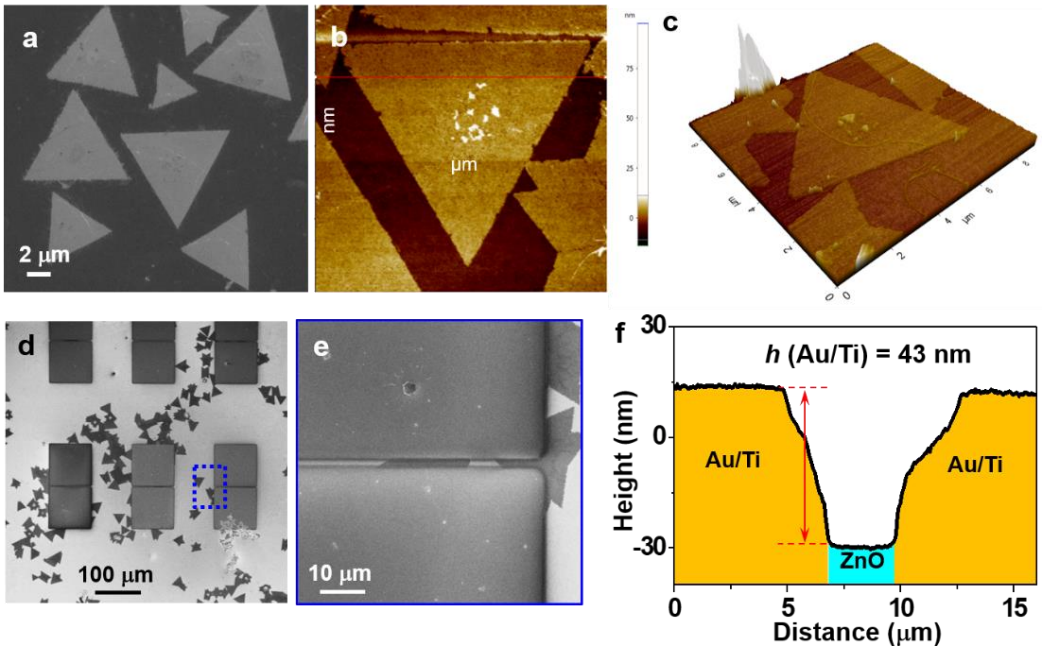

Figure S1. (a) Triangular ZnO nanosheets on Si substrate. (b, c) AFM of triangular ZnO nanosheets (d) Large scale SEM image of memory devices on Si substrate with 50 nm thermal oxide. (e) Enlarged SEM image showing the two Ti/Au electrodes and ZnO nanosheets. (f) Height profile along the red dashed line in (e), illustrating the configuration of the device. The thickness of Ti/Au electrodes were ~43 nm, and the channel width was ~3.1 μm.

S3. Device characterization without amorphous Al_2O_3 coating and leakage current with amorphous Al_2O_3 coating.

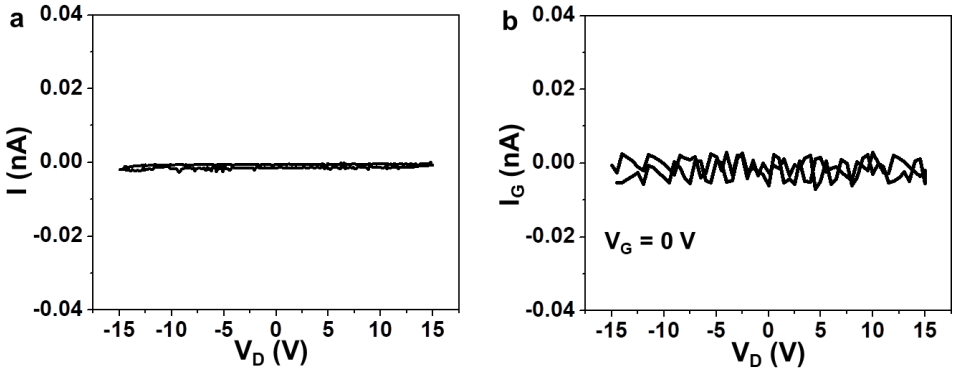

Figure S2. (a) Drain current versus drain voltage of the device without amorphous Al_2O_3 coating, showing there was no current signal in the bias range of −15 V to 15 V. (b) Gate current versus drain voltage curve of the device with amorphous Al_2O_3 coating. During the memristive measurement, the leakage current that flowed through the substrate (SiO_2/Si) was also monitored through a backgate on the device. As shown in Figure S2b, the leakage current was negligible when sweeping the voltage from -15 V to 15 V.

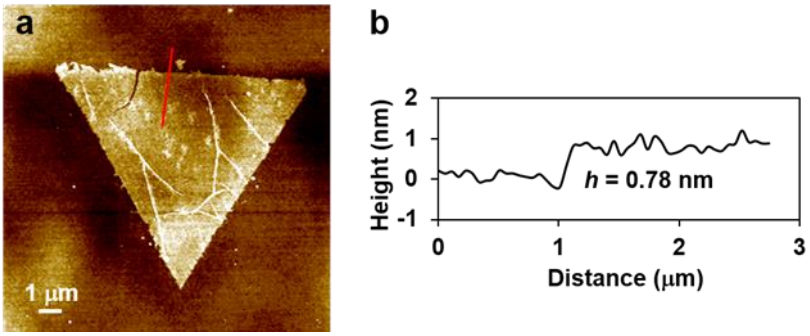

Figure S3. (a) AFM topography image of ZnO nanosheet coated by 5 nm Al_2O_3 through atomic layer deposition. (b) Height profile showing the thickness of 0.78 nm for the nanosheet in (a).

S4. Device characterization with Al_2O_3 coating but without ZnO nanosheets to illustrate that the Al_2O_3 is not contributing to the memristive behavior.

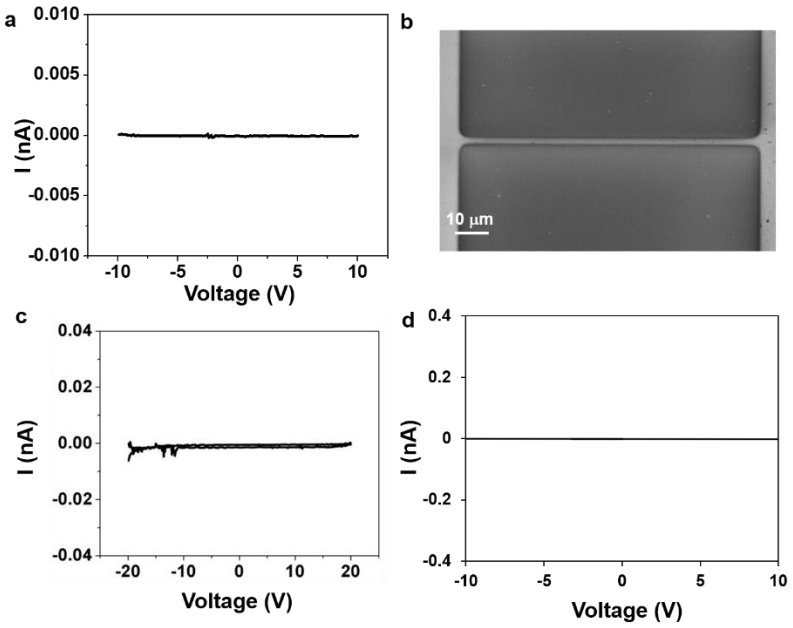

Figure S4. (a) Drain current versus drain voltage when there was no ZnO nanosheet (with Al_2O_3 coating), showing no current. (b) The corresponding SEM image without ZnO nanosheet (with Al_2O_3 coating) between electrodes. (c) Drain current versus drain voltage of the device with only amorphous Al_2O_3 coating, showing there was no current signal in the bias range from -20 V to 20 V. (d) The I-V curve after 2D ZnO/Al_2O_3 heterostructure was destroyed. The Al_2O_3 layer was deposited uniformly on both the electrodes and the area between the electrodes. The Al_2O_3 layer had no contribution to the memristive behavior. This could be attributed to the large electrode gap (3 μm) and the ultrasmall thickness (5 nm) of the Al_2O_3 film.

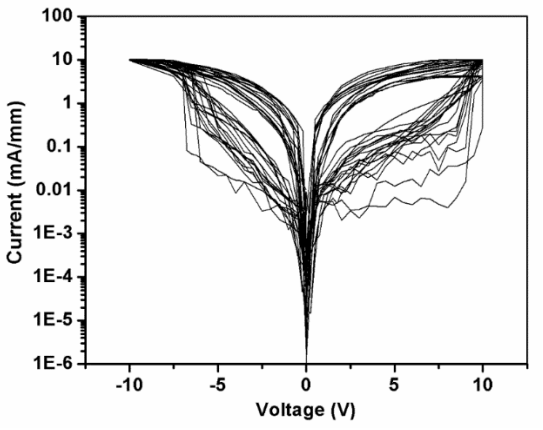

Figure S5. The logarithm scale of I-V curves of ZnO/Al_2O_3 memristor for 20 cycles without using pulse.

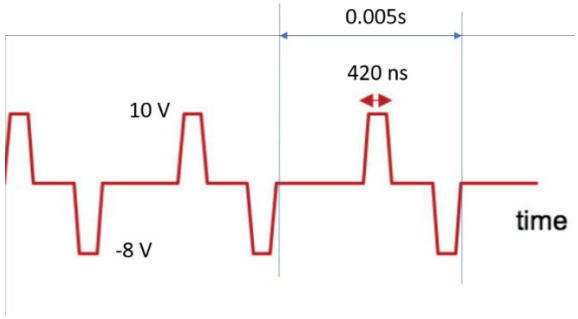

Figure S6. Pulse signal for endurance.

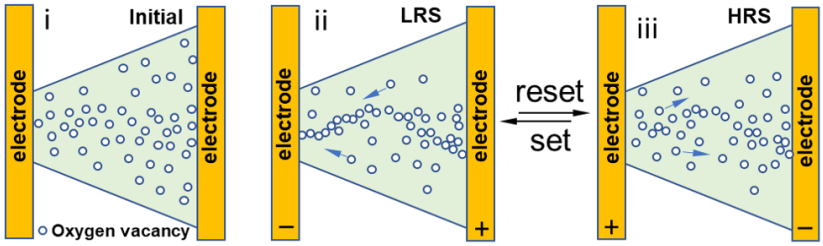

Figure S7. Schematic diagram for the mechanism of resistive switching. (i) the initial state of oxygen vacancies in ZnO nanosheets after Al_2O_3 coating. (ii) Under the set voltage, the oxygen vacancies migrated toward the cathode (oxygen ions (O^{2-}) toward the anode) and a conductive filament formed. (iii) Under the reset voltage, the filament ruptured and the device reset back to the HRS state

Table S1. Carrier mobility of metal oxides

Material	**Carrier mobility** ($cm^2\ V^{-1}\ s^{-1}$)
$Ti_{0.91}O_2$ [3]	500
2D $MoO_{(3-x)}$ [4]	> 1100
2 $CdO{\cdot}GeO_2$ thin film [5]	10
$InGaO_3(ZnO)_5$ thin film [6]	>10
In-Ga-Zn-O thin film [7]	>10

Single layer MoS_2 with HfO_2[8]	~200
alternating layers of In_2O_3, Ga_2O_3, and ZnO[9]	25-45
Si-doped Ga_2O_3 [10]	~200
ZnO thin film[11]	400
n-type ZnO film[12]	95.6
Bulk ZnO (50K)[13]	205 (2000)
MoS_2 with Al_2O_3[14]	41.2
In_2O_3 nanowire[15]	70–250

Table S2. Comparison of the memristive performance of ZnO devices

Devices	Maximum operation current (mA)	V_s (V)	V_R (V)	Electric filed ($x10^7$ V/m)	ON/OFF ratio (times)
1	0.1	12	-5	0.4	$2*10^3$
2	0.1	11	-10	0.37	$2*10^3$
3	0.03	15	-15	0.5	$5*10^2$
4	0.03	7.5	-5	0.25	$1*10^3$
5	0.03	9	-7.5	0.3	$1*10^3$
6	0.03	8.75	-7.44	0.29	$1*10^3$

Table S3. Summary of representative 2D resistive switching devices

2D materials	structure	Vset	Vreset	distance	Set field /$V \cdot m^{-1}$	Current	Ref.
MoS_2	Au/MoS_2/Au	80	-80	5 μm	$1.6*10^7$	~0.2 mA	[16]

$MoS_{2-x}O_x$	Graphene /$MoS_{2-x}O_x$/ Graphene	3.5	-4.8	40 nm	$8.75*10^7$	~1 mA	[2]
MoS_2	Au/Ti/MoS_2/Ti/Au	15	-15	2 µm	$0.75*10^7$	0.2 mA	[17]
MoS_2	Au/MoS_2/Au	1	-1.25	0.7 nm		10 mA	[18]
ZnO/Al_2O_3	Au/Ti/ZnO/Al_2O_3/Ti/Au	8.75	-7.44	3 µm	$0.29*10^7$	0.03 mA	This work
$WO_3 \cdot 2H_2O$	Cu/$WO_3 \cdot H_2O$/ITO-PET	1	-1.14	600 nm	$0.16*10^7$	10 mA	[19]
MoO_x/MoS_2	Ag/MoO_x/MoS_2/Ag	0.15	-0.1	100 nm	$0.16*10^7$	10 mA	[20]
Graphene Oxide	Al/G-O/Al/	2.5	-3	15 nm	$16*10^7$	0.05 mA	[21]
h-BN	Ti/thin h-BN/Cu	0.4	-0.8	2 nm	$20*10^7$	2 mA	[22]

References:

[1] X. Yin, Y. Wang, R. Jacobs, Y. Shi, I. Szlufarska, D. Morgan, X. Wang, *Nano Lett.* **2019**, *19*, 7085.

[2] M. Wang, S. Cai, C. Pan, C. Wang, X. Lian, Y. Zhuo, K. Xu, T. Cao, X. Pan, B. Wang, S.-J. Liang, J. J. Yang, P. Wang, F. Miao, *Nat. Electron.* **2018**, *1*, 130.

[3] M. Osada, T. Sasaki, *Adv. Mater.* **2012**, *24*, 210.

[4] S. Balendhran, J. Deng, J. Z. Ou, S. Walia, J. Scott, J. Tang, K. L. Wang, M. R. Field, S. Russo, S. Zhuiykov, M. S. Strano, N. Medhekar, S. Sriram, M. Bhaskaran, K. Kalantar-zadeh, *Adv. Mater.* **2013**, *25*, 109.

[5] S. Narushima, M. Orita, M. Hirano, H. Hosono, *Phys. Rev. B* **2002**, *66*, 035203.

[6] K. Nomura, T. Kamiya, H. Ohta, K. Ueda, M. Hirano, H. Hosono, *Appl. Phys. Lett.* **2004**, *85*, 1993.

[7] K. Nomura, H. Ohta, A. Takagi, T. Kamiya, M. Hirano, H. Hosono, *Nature* **2004**, *432*, 488.

[8] B. Radisavljevic, A. Radenovic, J. Brivio, V. Giacometti, A. Kis, *Nat. Nanotech.* **2011**, *6*, 147.

[9] Y.-H. Lin, H. Faber, J. G. Labram, E. Stratakis, L. Sygellou, E. Kymakis, N. A. Hastas, R. Li, K. Zhao, A. Amassian, N. D. Treat, M. McLachlan, T. D. Anthopoulos, *Adv. Sci.* **2015**, *2*, 1500058.

[10] Y. Kang, K. Krishnaswamy, H. Peelaers, C. G. Van de Walle, *J. Phys. Condens. Matter.* **2017**, *29*, 234001.

[11] I. Gonzalez-Valls, M. Lira-Cantu, *Energy Environ. Sci.* **2009**, *2*, 19.

[12] F. X. Xiu, Z. Yang, L. J. Mandalapu, D. T. Zhao, J. L. Liu, W. P. Beyermann, *Appl. Phys. Lett.* **2005**, *87*, 152101.

[13] D. C. Look, D. C. Reynolds, J. R. Sizelove, R. L. Jones, C. W. Litton, G. Cantwell, W. C. Harsch, *Solid State Commun.* **1998**, *105*, 399.
[14] S. Y. Kim, S. Park, W. Choi, *Appl. Phys. Lett.* **2016**, *109*, 152101.
[15] H. Huang, B. Liang, Z. Liu, X. Wang, D. Chen, G. Shen, *J. Mater. Chem.* **2012**, *22*, 13428.
[16] V. K. Sangwan, H.-S. Lee, H. Bergeron, I. Balla, M. E. Beck, K.-S. Chen, M. C. Hersam, *Nature* **2018**, *554*, 500.
[17] D. Li, B. Wu, X. Zhu, J. Wang, B. Ryu, W. D. Lu, W. Lu, X. Liang, *ACS Nano* **2018**, *12*, 9240.
[18] R. Ge, X. Wu, M. Kim, J. Shi, S. Sonde, L. Tao, Y. Zhang, J. C. Lee, D. Akinwande, *Nano Lett.* **2018**, *18*, 434.
[19] L. Liang, K. Li, C. Xiao, S. Fan, J. Liu, W. Zhang, W. Xu, W. Tong, J. Liao, Y. Zhou, B. Ye, Y. Xie, *J. Am. Chem. Soc.* **2015**, *137*, 3102.
[20] A. A. Bessonov, M. N. Kirikova, D. I. Petukhov, M. Allen, T. Ryhänen, M. J. A. Bailey, *Nat. Mater.* **2014**, *14*, 199.
[21] H. Y. Jeong, J. Y. Kim, J. W. Kim, J. O. Hwang, J.-E. Kim, J. Y. Lee, T. H. Yoon, B. J. Cho, S. O. Kim, R. S. Ruoff, S.-Y. Choi, *Nano Lett.* **2010**, *10*, 4381.
[22] C. Pan, Y. Ji, N. Xiao, F. Hui, K. Tang, Y. Guo, X. Xie, F. M. Puglisi, L. Larcher, E. Miranda, L. Jiang, Y. Shi, I. Valov, P. C. McIntyre, R. Waser, M. Lanza, *Adv. Funct. Mater.* **2017**, *27*, 1604811.